Medicinal Chemistry Research (2019) 28:246–259
https://doi.org/10.1007/s00044-018-2280-z

MEDICINAL CHEMISTRY RESEARCH

ORIGINAL RESEARCH

Studies of NMR, molecular docking, and molecular dynamics simulation of new promising inhibitors of cruzaine from the parasite *Trypanosoma cruzi*

Renato A. Costa[1,2] · Jorddy N. Cruz[3] · Fabiana C. A. Nascimento[2] · Sebastião G. Silva[2] · Silvana O. Silva[2] · Marlice C. Martelli[2] · Samira M. L. Carvalho[2] · Cleydson B. R. Santos[4] · Antonio M. J. C. Neto[3] · Davi S. B. Brasil[2]

Received: 8 August 2018 / Accepted: 14 December 2018 / Published online: 25 December 2018

Abstract
Cruzaine is the major cysteine protease of *Trypanosoma cruzi*. Cruzaine is involved throughout the parasite's life cycle in host cells, and is a promising target in the search for new antichagasic agents. Quantum chemical calculations based on density functional theory (DFT B3LYP/cc-pVDZ) were performed to obtain nuclear magnetic resonance data and to optimize the geometry of four dihydrochalcones. The results showed good agreement with the experimental data and were used to suggest the relative stereochemistry of one of the four dihydrochalcones studied. In addition, we evaluated the interaction of cruzaine with these new inhibitors. We used molecular dynamics simulations, free energy calculations, and a per-residue energy decomposition method. It was observed that these molecules are capable of interacting with residues important for enzymatic activity, like Cys25, His161, and Asp160. The ranking of the inhibitors obtained from the binding free energy calculations is in agreement with that experimentally reported. The evaluation of the energy components involved in these calculations demonstrated that the van der Waals term is the major contributor to the drug–receptor stabilizing interactions.

Keywords RMN · New inhibitors · Cruzaine · Docking · Molecular dynamics

Introduction

Chagas disease is a disease caused by the flagellate protozoan *Trypanosoma cruzi (T. cruzi)* (Chagas and Chagas 1909). This disease, in many Latin American countries, is a public health problem because of the high fatality rate (Chatelain 2017).

More than 100 years after its discovery, Chagas disease continues to be neglected. The infection by the *T. cruzi* parasite affects about 6 million people, mainly in Latin America (Pérez-Molina and Molina 2018). This disease can be transmitted orally, by blood transfusion, via placental or congenital transmission, through the birth canal at the time of birth, in laboratory accidents, by handling infected animals, by raw meat intake, through organ transplantation, and via sexual transmission (Coura 2015).

Currently, only two drugs are clinically available for the chemotherapy of Chagas disease: benzonidazole and nifurtimox. Both are options for patients in the acute phase of the disease but are less effective in the chronic phase (Morillo et al. 2015). Another reason why the search for new antichagastic agents is necessary is because parasites, through different mechanisms, develop resistance to commonly used drugs (Carneiro et al. 2017).

From the sequencing of the *T. cruzi* genome, it was possible to identify several promising biological targets, and

Supplementary information The online version of this article (https://doi.org/10.1007/s00044-018-2280-z) contains supplementary material, which is available to authorized users.

✉ Jorddy N. Cruz
jorddynevescruz@gmail.com

[1] Federal Institute of Pará, Parauapebas, PA 68515-000, Brazil

[2] Post-Graduate Program in Chemistry, Federal University of Pará, Belém, PA 66075-110, Brazil

[3] Laboratory of Preparation and Computation of Nanomaterials, Federal University of Pará, Belém, PA 66075-110, Brazil

[4] Laboratory of Modeling and Computational Chemistry, Federal University of Amapá, Macapá, AP 68902-280, Brazil

most of these were from enzymes (Magalhaes Moreira et al. 2014). Among these enzymes, the major cysteine trypanosomal cysteine protease is involved in the invasion, differentiation, and proliferation processes of the parasite in host cells (Massarico Serafim et al. 2014).

Cruzaine is expressed at all stages of parasite development (Caputto et al. 2011). This enzyme has the interaction site divided into four subsites (S1, S1', S2, and S3) that are targeted for the development of new inhibitors (McGrath et al. 1995). The catalytic cysteine, Cys25, and other two residues, His159 and Gln19, which form the catalytic triad of the enzyme, are present in the sites S1 and S1'; these latter two amino acids are part of the region known as oxyion cavity that plays a role in the mechanism of the reaction catalyzed by the enzyme (Turk et al. 1998). Subsites S1, S1', and S2 are responsible for enzyme–substrate interactions while S3 accounts for the enzymatic specificity (Farady and Craik 2010).

In the present study, theoretical methods at the DFT/B3LYP /cc-pVDZ level were used to determine the structural (geometric) and spectroscopic data (1H and 13C NMR) of four dihydrochalcones. The nuclear magnetic resonance (NMR) calculation results showed good agreement with the experimental data and were used to suggest the relative stereochemistry of dihydrochalcone 4, which could not be determined experimentally. Besides that, molecular docking studies were performed using four dihydrochalcones isolated from *Metrodorea stipularis* (Burger et al. 2014), reported as promising inhibitors of cruzaine (Fig. 1).

To evaluate the mechanism of the interaction of cruzaine with these new inhibitors, molecular dynamics (MD) simulations and free energy calculations using the molecular mechanics generalized born surface area (MM/GBSA) method were employed. We also explored the importance of the different residues of the cross-linked binding site on the drug–receptor interactions by applying a per-residue binding free energy decomposition technique. In addition, we also investigated the chemical nature of the interactions of these residues with the inhibitors.

Methodology

Computational methods

Initially, structural optimization of dihydrochalcones **1**, **2**, and **3** was performed, and, later, the vibrational analyses confirmed the stationary points using the density functional theory (DFT) method at the level of B3LYP/cc-pVDZ (Lee et al. 1988; Borges et al. 2016). The representative local minimum energy conformations were used as input in the calculations of the chemical displacements of 1H and 13C, using DFT with the gauge invariant atomic orbital method (DFT-GIAO) (Rauhut et al. 1996) approximation at the B3LYP/cc-pVDZ level of theory under the influence of the acetone solvent modeled using the continuous polarization model (Miertuš et al. 1981), to prove the effectiveness of the method employed. After proving the efficiency of the computational method, it was used to elucidate the stereochemistry of dihydrochalcone **4**, which presented two structural possibilities: **4A** and **4B**, as can be observed in Fig. 2.

The two structural possibilities were optimized at the B3LYP level together with the basis set cc-pVDZ, by

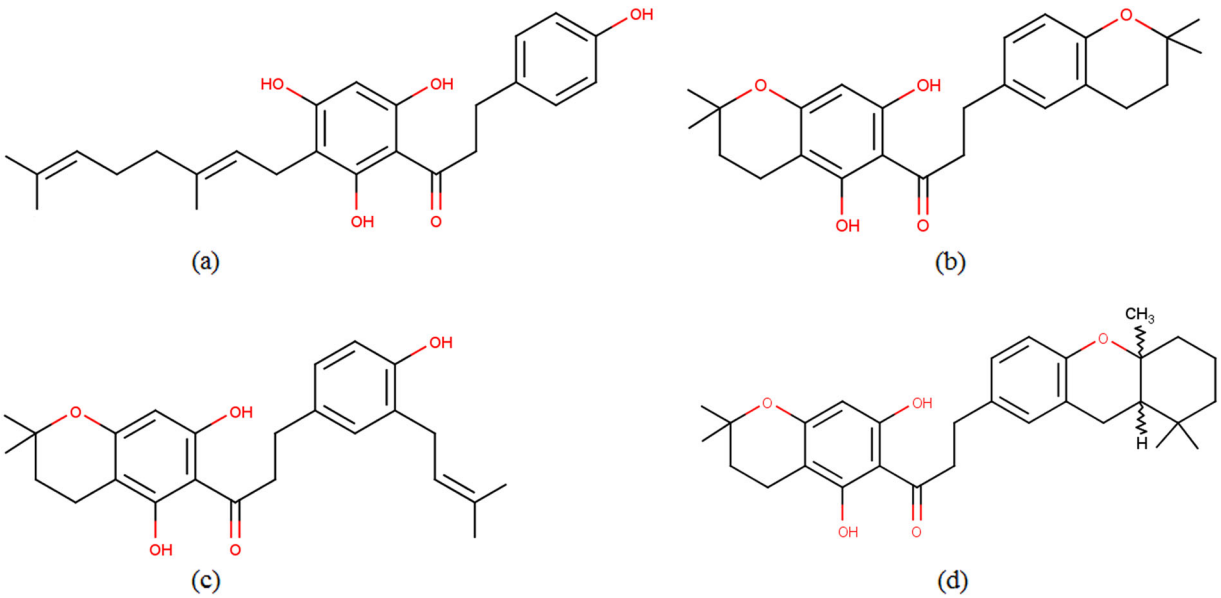

Fig. 1 Chemical structure of the compounds. **a** Dihydrochalcone **1**, **b** Dihydrochalcone **2**, **c** Dihydrochalcone **3**, and **d** Dihydrochalcone **4**

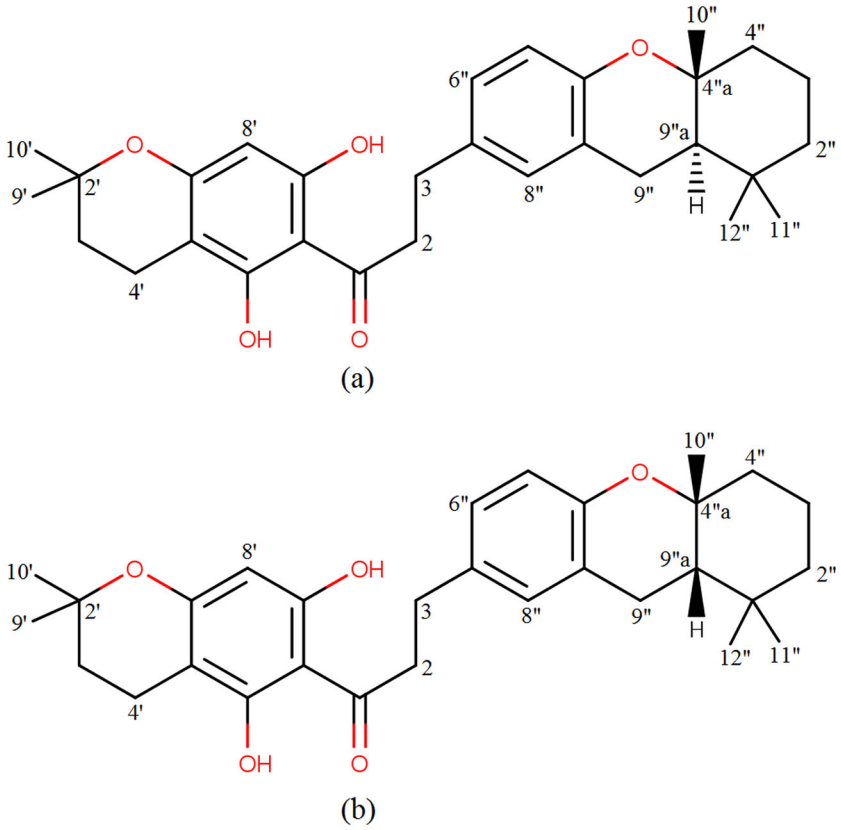

Fig. 2 Structural possibilities of Dihydrochalcone **4**. **a** Dihydrochalcone **4A** and **b** Dihydrochalcone **4B**

adjusting such molecules to a minimum local energy conformation, and minimum energy structures were guaranteed by the absence of any imaginary frequency. To obtain the chemical displacements of 13C and 1H, the GIAO method was used (Gauss and Stanton 1995). The calculations were carried out under the influence of the methanol solvent, modeled by the PCM, using as input the optimized structures at the B3LYP/cc-pVDZ level (Kaur et al. 2015; Khan et al. 2017).

Statistical analysis

The NMR data were analyzed using linear regression, and the most-relevant parameters were: degree of adjustment (R^2), standard deviation (s), degree of significance (F), and predictability (Q^2 and s_{PRESS}). The software MINITAB 14 was used in the statistical analysis (Wild 2005). Other statistical parameters were determined to evaluate the quality of the calculations, but none of them can be considered satisfactory if analyzed individually: coefficients a and b of the linear regression $\delta_{calc} = a + b\delta_{exp}$; average absolute error (AAE), defined as $AAE = \Sigma_n \mid \delta_{calc} - \delta_{exp} \mid /n$; and corrected mean absolute error (CMAE), defined by $CMAE = \Sigma_n \mid \delta_{corr} - \delta_{exp} \mid /n$, onde $\delta_{corr} = (\delta_{calc} - a)/b$ (Cimino et al. 2004; Brasil et al. 2008). In addition, the predicted values for δ were determined by applying the mathematical models obtained and comparing them with the experimental values.

The equations obtained by the linear-regression procedure were tested for their predictability power using a cross-validation procedure. Cross-validation is a practical and reliable method of testing for significance. The so-called "leave-one-out" approach consists of developing a series of models omitting one sample at a time. After the development of each model, the omitted data are predicted, and the difference between true and predicted values ($\hat{y}$) are calculated. The sum of the squares of these differences is determined. Finally, the performance of the model (its predictive ability) can be given by the sum of the square of the prediction errors (PRESS) e S_{PRESS} (standard deviation of cross-validation) (Moreira et al. 2008):

$$\begin{aligned} \text{PRESS} &= \textstyle\sum_{i=1}^{n} (y_i - \hat{y}_i)^2 \\ {}^{s}\text{Press} &= \frac{\sqrt{PRESS}}{n-k-1} \end{aligned} \quad (1)$$

where y is the experimental value, $\hat{y}$ is the predicted value, n is the number of samples used to obtain the model, and k is the number of NMR parameters.

The predictive ability of the models was also quantified in terms of Q^2, which is defined as:

$$Q^2 = 1.0 - \frac{\sum_{i=1}^{n}(y_i - \hat{y}_i)^2}{\sum_{i=1}^{n}(y_i - \overline{y}_i)^2} \quad (2)$$

onde, $\overline{y} = y_{average}$.

Molecular docking

The chemical structures of the four dihydrochalcones were designed using the GaussView 5 software (Dennington et al. 2015) and then optimized with the DFT method at the B3LYP/cc-pVDZ level using the Gaussian 09 software (Frisch et al. 2009). Molecular virtual docker (MVD) 5.5 (Thomsen and Christensen 2006) and the crystallographic model of the cross-enzyme code ID: 1ME3 (Huang et al. 2003) in the protein data bank were used for the molecular docking simulations. The receptor and linkers were prepared using a standard MVD preparation module. For each complex, hydrogen atoms were added, and the program's standard partial atomic charges were employed. The docking calculations were performed using the MolDock scoring function, with a grid resolution of 0.3 Å. The region of the active site of the enzyme was defined as a spherical region of 10 Å, covering all amino acid residues of the cross-linked active site, with the center at $x = 2.32$, $y = 12.32$, and $z = 5.98$. For each complex, the calculations were performed generating different conformations using the MolDock optimizer algorithm.

Molecular dynamics simulation

The protonation states of the amino acid residues of the protein were determined from the results obtained with the PDB2PQR server (Dolinsky et al. 2004).

The atomic charges of the inhibitor molecules were calculated using the restrained electrostatic potential (RESP) protocol at the HF/6-31G* level of theory (Cornell et al. 1993; Wang et al. 2000) using the Gaussian 09 software. We used the Antechamber module of Amber 16 (Case et al. 2005; Cruz et al. 2018) to create parameters compatible with the general Amber force field (GAFF) (Wang et al. 2004) for the inhibitors.

The tLEaP module was used to construct the systems and to add the absent hydrogens. The simulations were carried out using an explicit solvent representation in which the water molecules where described by the TIP3P model (Jorgensen et al. 1983). The force field used for all atomic simulations was ff14SB (Maier et al. 2015).

Then, each system was solvated in an octahedron periodic box, and a 12 Å cutoff radius was applied. To conclude this step, counterions were added to neutralize the charge of the enzyme-inhibitor system.

Prior to the MD production simulations, the systems were subjected to energy minimization, heating, and equilibration.

Four steps were performed to minimize the energy of the systems. In each step, 5000 cycles were performed with the steepest descent method and conjugate gradient algorithm. In the first stage, the solute was fixed with a harmonic force constant of 100 kcal/(mol Å^2). In the following steps, this harmonic force constant was gradually reduced until it reached zero in the last step so that the whole complex (solute, water, and counterions) was free to move.

The systems were heated to 300 K in four steps of 600 ps. In the two initial steps, a harmonic force constant of 25 kcal/(mol Å^2) was applied to restrict the solute. There were no restrictions in the two final stages. A Langevin thermostat (Izaguirre et al. 2001) with a collision frequency of 3.0 ps^{-1} was used.

To equilibrate the system, a 5 ns MD simulation at a constant temperature of 300 K and without any restriction was performed.

The calculation of the electrostatic interactions was performed using the particle mesh Ewald method (Darden et al. 1993), and the SHAKE algorithm (Ryckaert et al. 1977) was used to restrict the bond lengths involving hydrogen atoms.

After all these steps, 100 ns MD production simulations were carried out on all the systems.

MM/GBSA calculations

The MM/GBSA method was applied to estimate binding free energies (ΔG_{bind}) (Kollman et al. 2000; Genheden and Ryde 2015). To this end, 1000 snapshots were extracted from the last 5 ns of every MD simulation.

The ΔG_{bind} can be calculated according to the equations:

$$\Delta G_{\text{bind}} = G_{\text{complex}} - \left(G_{\text{protein}} + G_{\text{ligand}}\right) \quad (3)$$

$$\Delta G_{\text{bind}} = \Delta H - T\Delta S \approx \Delta E_{\text{MM}} + \Delta G_{\text{solv}} - T\Delta S \quad (4)$$

$$\Delta E_{\text{MM}} = \Delta E_{\text{internal}} + \Delta E_{\text{electrostatic}} + \Delta E_{\text{vdw}} \quad (5)$$

$$\Delta G_{\text{solv}} = \Delta G_{\text{GB}} + \Delta G_{\text{nonpol}} \quad (6)$$

Where ΔG_{bind} is the inhibitor-protein binding free energy resulting from the sum of the molecular mechanics energy (ΔE_{MM}), desolvation free energy (ΔG_{solv}), and the entropic term ($-T\Delta S$). The gas-phase molecular mechanics energy (ΔE_{MM}) can be described by the sum of the internal energy contributions ($\Delta E_{\text{internal}}$, sum of the energies due to the bonds, angles, and dihedrals), electrostatic contributions ($\Delta E_{\text{electrostatic}}$), and van der Waals term (ΔE_{vdw}). The desolvation free energy (ΔG_{solv}) is the sum of the polar (ΔG_{GB}) and non-polar (ΔG_{nonpol}) contributions. The polar desolvation term was calculated using the implicit generalized Born (GB) approach.

Per-residue energy decomposition

A per-residue energy decomposition method was used to determine the total energy contribution of each residue to

Table 1 13C and 1H experimental (Exp.), theoretical (DFT), residues and predicted (by linear models) data for the structure of dihydrochalcone **1** (in ppm)

Position	Exp.	13C			Exp.	1H		
		Calc.	Res	Pred.		Calc.	Res	Pred.
C1	134.4	133.78	0.62	136.08				
C2	130.1	129.55	0.55	131.65	7.09	6.89	0.2	7.19
C3	115.8	113.05	2.75	114.36	6.75	6.48	0.27	6.77
C4	156.4	153.41	2.99	156.63				
C5	115.8	112.03	3.77	113.29	6.75	6.32	0.43	6.6
C6	130.1	126.13	3.97	128.06	7.09	7.02	0.07	7.33
C1'	102.1	107.38	5.28	108.43				
C2'	162.6	156.37	6.23	159.74				
C3'	107.8	102.8	5	103.62				
C4'	165.4	156.32	9.08	159.68				
C5'	94.9	91.17	3.73	91.45	6.07	5.5	0.57	5.76
C6'	160.4	155.53	4.87	158.86				
C1"	21.8	24.63	2.83	21.75	3.26	2.74	0.52	2.9
C2"	124	122.42	1.58	124.18	5.27	4.97	0.3	5.21
C3"	133.5	139.72	6.22	142.3				
C4"	16.1	15.78	0.32	12.48	1.77	1.75	0.02	1.88
C5"	40.5	47.14	6.64	45.32	1.92	1.78	0.14	
C6"	27.4	32.08	4.68	29.54	2.1	1.96	0.14	
C7"	125.1	126.2	1.1	128.14	5.1	5.19	0.09	5.43
C8"	131.4	135.23	3.83	137.59				
C9"	25.8	27.59	1.79	24.85	1.62	1.58	0.04	1.7
C10"	17.7	18.05	0.35	14.85	1.56	1.51	0.05	1.63
CO	205.5	198.3	7.2	203.66				
Cα	46.8	47.12	0.32	45.3	2.89	2.93	0.04	3.1
Cβ	30.7	32.8	2.1	30.3	3.34	2.91	0.43	3.07

Table 2 13C and 1H NMR (Exp.), theoretical (DFT), residues and predicted (by linear models) data for the structure of dihydrochalcone **2** (in ppm)

Position	Exp.	13C			Exp.	1H		
		Calc.	Res	Pred.		Calc.	Res	Pred.
C1	204.7	199.27	5.43	204.78				
C2	45.5	54.24	7.74	49.92	3.3	2.8	0.5	3.07
C3	29.7	36.27	6.57	31.92	2.83	2.62	0.21	2.89
C2'	75.6	79.25	3.65	77.37				
C3'	31.2	34.81	3.61	30.35	1.76	1.73	0.03	1.97
C4'	16.2	18.97	2.77	13.59	2.53	2.26	0.27	2.51
C4'a	104.8	99.84	4.96	99.16				
C5'	157	156.49	0.51	159.12				
C6'	100	108.56	8.56	108.39				
C7'	162.2	155.29	6.91	158.14				
C8'	94.5	92.75	1.75	91.82	5.92	5.44	0.48	5.8
C8'a	165.2	156.94	8.56	159.89				
C9'	25.5	31.47	5.97	26.84	1.22	1.33	0.11	1.56
C10'	25.5	24.17	1.33	19.1	1.22	1.15	0.07	1.36
C2"	73.2	77.87	4.67	76.04				
C3"	32.4	35.52	3.12	31.14	2.69	1.54	1.15	1.77
C4"	22.1	25.8	3.7	20.82	2.69	2.45	0.24	2.71
C4"a	120	121.85	1.85	122.68				
C5"	126.8	129.18	2.38	127.71	6.91	6.29	0.62	6.68
C6"	132.2	133.46	1.26	134.99				
C7"	128.1	126.59	1.51	130.45	6.93	6.87	0.06	7.28
C8"	116.8	116.02	0.78	116.5	6.56	6.44	0.12	6.84
C8"a	151.9	152.07	0.17	154.73				
C9"	25.5	24.51	0.99	19.45	1.33	1.1	0.23	1.31
C10"	25.5	31.89	6.99	27.28	1.33	1.26	0.07	1.48

the drug–receptor interaction and also to investigate the chemical nature of its interactions (Gohlke et al. 2003).

The interaction energy between an inhibitor and every residue in the enzyme can be described, according to the equation below, as a sum of four terms: van der Waals (ΔE_{vdw}) and electrostatic (ΔE_{ele}) contributions in the gas-phase, and polar (ΔG_{pol}) and nonpolar solvation (ΔG_{nonpol}) contributions:

$$\Delta G_{inhibitor-residue} = \Delta E_{vdw} + \Delta E_{ele} + \Delta G_{pol} + \Delta G_{nonpol} \quad (7)$$

Results and discussion

NMR spectra and statistical analysis

The theoretical NMR data of 1H and 13C were calculated for dihydrochalcones **1**, **2**, and **3** and tetramethylsilane (TMS) (internal standard, shielding constants of 31.2969 for 1H and 192.5621 for 13C). The NMR chemical shifts 1H and 13C, the experimental (Burger et al. 2014), theoretical, and predicted values, and the difference between experimental and theoretical chemical shifts in 1, 2, and 3 are presented in Tables 1–3, respectively. The most-relevant statistical parameters are presented in Table 4.

Figure 3 shows the correlation between the calculated and experimental chemical shifts of 13C (**a**) and 1H (**b**).

Statistical analysis revealed that all linear models had a good linear correlation and satisfactory results after the cross-validation procedure for the 1H and 13C NMR data of the three structures. These results confirm the relevance of the theoretical data used to calculate the chemical shifts of these compounds.

The statistical data show that, in general, the regression model of 1H and 13C NMR data of the structures is significant and well adjusted. This analysis indicates that there is a linear agreement between the theoretical chemical shift

data of 1H and 13C NMR obtained in relation to the experimental values for the dihydrochalcones studied, because they are quantitatively similar to the experimental chemical shifts mentioned in the literature, showing that the theoretical method B3LYP/cc-pV-DZ, applied here, can be a tool that effectively helps the use of NMR techniques.

The values of the chemical shifts calculated at the level of B3LYP/cc-pV-DZ were close to the experimental ones, as can be observed in Tables 1–3, presenting low residual values (difference between experimental and theoretical

Table 3 13C and 1H NMR (Exp.), theoretical (DFT), residues and predicted (by linear models) data for the structure of dihydrochalcone **3** (in ppm)

Position	Exp.	13C			Exp.	1H		
		Calc.	Res	Pred.		Calc.	Res	Pred.
C1	204	196.13	7.87	200.53				
C2	45.5	53.64	8.14	50.02	3.25	2.59	0.66	2.71
C3	30.2	34.62	4.42	29.93	2.82	2.66	0.16	2.79
C2'	75.6	79.32	3.72	77.14				
C3'	31.3	34.76	3.46	30.08	1.76	1.72	0.04	1.82
C4'	15.9	19.16	3.26	13.59	2.55	2.33	0.22	2.45
C4'a	104.8	99.81	4.99	98.79				
C5'	162	155.95	6.05	158.1				
C6'	100	108.18	8.18	107.63				
C7'	156	155.77	0.23	157.9				
C8'	94.1	94.11	0.01	92.76	5.87	5.63	0.24	5.83
C8'a	164	157.72	6.28	159.96				
C9'	25	24.28	0.72	19	1.33	1.18	0.15	1.26
C10'	25	31.48	6.48	26.61	1.33	1.33	0	1.46
C1"	132.2	132.72	0.52	133.55				
C2"	128.7	129.05	0.35	129.67	6.87	6.64	0.23	6.86
C3"	126	127.05	1.05	127.56				
C4"	152	154.85	2.85	156.93				
C5"	114.3	114.53	0.23	114.34	6.64	6.39	0.25	6.61
C6"	125.9	127.83	1.93	128.39	6.83	6.78	0.05	7.01
C1"'	27.7	35.93	8.23	31.31	3.25	3.19	0.06	3.33
C2"'	122.6	123.94	1.34	124.28	5.28	5.16	0.12	5.35
C3"'	131.4	142.16	10.76	143.52				
C4"'	16.4	18.5	2.1	12.9	1.68	1.7	0.02	1.8
C5"'	25.5	27.73	2.23	22.65	1.69	1.79	0.1	1.9

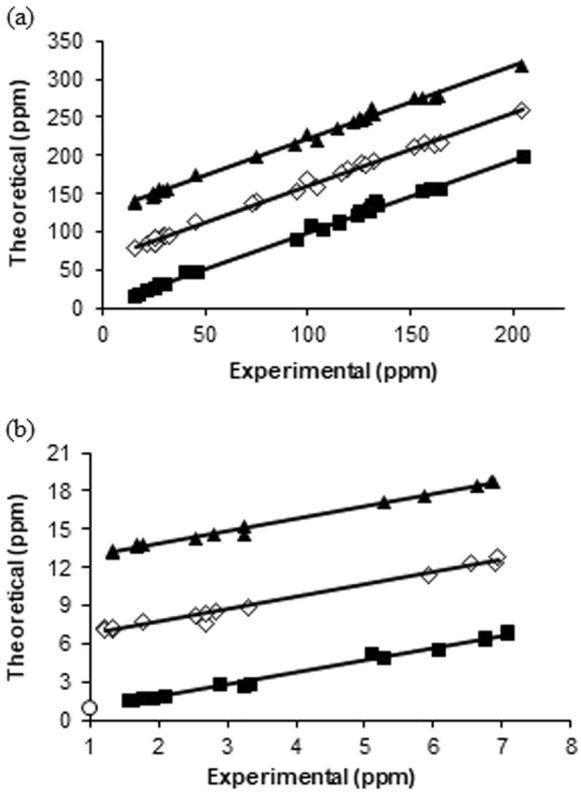

Fig. 3 Correlation between experimental and calculated chemical shifts of 13C **a** and 1H **b** for structures **1** (solid square), **2** (open square), and **3** (solid triangle). NMR data of structures **2** and **3** were displaced from 60 to 120 ppm (13C NMR) and from 6 to 12 ppm (1H NMR), respectively. For each set of data, the linear fitting is also reported as a dashed line

Table 4 Linear fit parameters to the NMR properties calculated for substances **1**, **2**, and **3**

Parameters	Dihydrochalcone 1		Dihydrochalcone 2		Dihydrochalcone 3	
	δ13C	δ1H	δ13C	δ1H	δ13C	δ1H
a	0.95	0.96	0.94	0.97	0.94	0.97
b	3.87	−0.06	6.16	−0.15	6.28	−0.05
EAM	3.51	0.22	3.79	0.27	3.82	0.17
EAMC	2.8	0.15	2.92	0.22	3.24	0.12
s	3.51	0.2	3.51	0.36	4.03	0.18
R^2	99.3%	98.88%	99.6%	98.02%	99.59%	99.31%
Q^2	99.52%	98.95%	99.53%	97.24%	99.38%	99.16%
F	5536.76	1547.03	5714.82	562.05	4351.36	1762.16
PRESS	326,659	0.670032	331,925	1.68	443.09	0.181872
S_{PRESS}	0.780.6	0.06	0.79	0.12	0.91	0.03

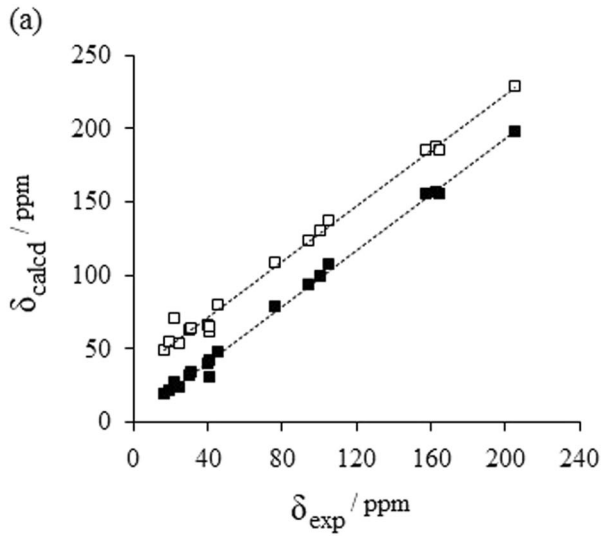

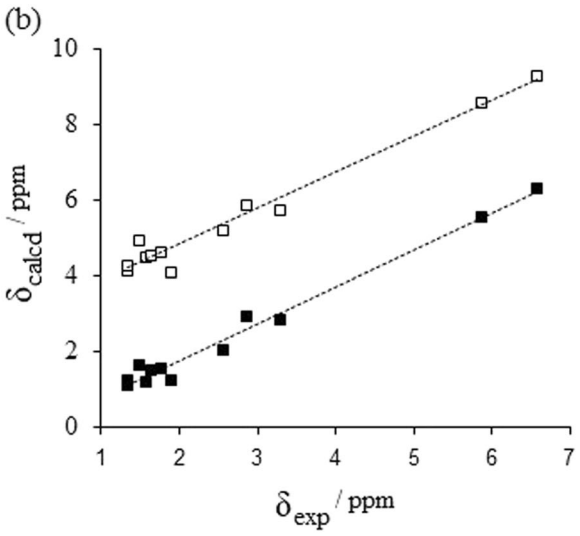

Fig. 4 Correlation between experimental and calculated chemical shifts of 13C **a** and 1H **b** for structures **4A** (solid square) and **4B** (open square). NMR data of the structures **4B** were displaced from 30ppm (13C NMR) and from 3 ppm (1H NMR), respectively. For each set of data, the linear fitting is also reported as a dashed line

chemical shifts) and similar to their respective predicted values (obtained with the linear models).

Statistical treatment based on simple linear-regression and cross-validation procedures reinforces the proximity between the theoretical and calculated data for the studied structures, reaching satisfactory correlation and predictability degrees, in addition to a high degree of significance, which generated linear models that confirm the efficiency of the computational method used, showing that the method can be applied to aid interpretation of experimental data to elucidate structures similar to the dihydrochalcones mentioned.

Thus, this theoretical method was used to suggest the relative stereochemistry of the C-4"a and C-9" positions of molecule **4**, which is not possible using the experimental data. Thus, it was necessary to design two structural possibilities of dihydrochalcone: **4A** and **4B**.

In Fig. 4, correlation plots obtained after linear-regression treatment of the theoretical 1H and 13C NMR data of substances **4A** and **4B** are shown, along with experimental NMR data of dihydrochalcone **4**. Afterward, the statistical parameters presented in Table 5 were evaluated to verify the degree of fit, significance, and predictability of the models, as well as which structure is better suited to the data obtained.

Analyzing the statistical data shows that the correlations obtained for the **4A** structure were those that presented the best parameters for δ_C ($R^2 = 99.60\%$; $S = 3.63$; $S_{PRESS} = 0.73$; $F = 6275.84$; $Q^2 = 99.49\%$) and for δ_H ($R^2 = 99.05\%$; $S = 0.19$; $S_{PRESS} = 0.05$; $F = 1923.91$; $Q^2 = 98.98\%$). That is, these linear models present the best adjustments, as well as the highest degree of significance and predictability, so

Table 5 Linear fit parameters to the NMR properties calculated for the possibilities **4A** and **4B**

Parameters	Dihydrochalcone 4A		Dihydrochalcone 4B	
	δ13C	δ1H	δ13C	δ1H
a	0.96	0.98	0.94	0.98
b	3.05	−0.16	4.49	−1.18
EAM	3.13	0.24	4.3	0.3
EAMC	2.62	0.15	3.73	0.22
s	3.63	0.19	5.15	0.33
R^2	99.6%	99.05%	98.92%	98.05%
Q^2	99.49%	98.98%	98.96%	97.12%
F	6275.84	1923.91	3028.16	672.29
PRESS	421,261	0.787435	843,671	21,697
S_{PRESS}	0.73	0.05	1.04	0.08

the results obtained with the theoretical calculations, treated from linear regression, indicate that substance **4A** is the most probable structure for compound 4.

The indication of structure **4A** was also suggested by analyzing the residue values near the C-4 "a and C-9" position A. Calculations of NMR chemical shifts of 13C and 1H in position C-4"a, when compared to the experimentally observed values for compound **4**, demonstrated the smallest residues, for structures **4A** [residue related to δ_C (Exp. – Calc.) in position C-4"a = 6.9 ppm]; e **4B** [residue related to δ_C (Exp. – Calc.) in position C-4"a = 7.7 ppm]; residue related to δ_C (Exp. – Calc.) in position C-9"a = 1.5 ppm; residue related to δ_H (Exp. – Calc.) in position C-9"a = 0.1 ppm]; and **4B** [residue related to δ_C (Exp. – Calc.) in position C-9"a = 2.6 ppm; residue related to δ_H (Exp. – Calc.) in position C-9"a = 0.44 ppm], **4A** [residue related to

Table 6 NMR (δH and δC) experimental (Exp.), theoretical (DFT), and predicted (by linear models) data for dihydrochalcone **4A** (in ppm)

Position	Exp.	13C			Exp.	1H		
		Calc.	Res	Pred.		Calc.	Res	Pred.
C1	204.7	197.71	6.99	202.14				
C2	45.4	47.78	2.38	46.44	3.28	2.85	0.43	3.06
C3	30	31.49	1.49	29.53	2.85	2.93	0.08	3.14
C1'a	162.2	157.42	4.78	160.3				
C2'	75.6	79.22	3.62	79.09				
C3'	31.2	34.6	3.4	32.76	1.77	1.54	0.23	1.73
C4'	16.2	18.88	2.68	16.43	2.56	2.04	0.52	2.24
C4'a	100	99.94	0.06	100.61				
C5'	157	155.54	1.46	158.35				
C6'	104.8	108.14	3.34	109.13				
C7'	164.5	155.49	9.01	158.3				
C8'	94	93.73	0.27	94.16	5.87	5.55	0.32	5.8
C9'	25	24.19	0.81	21.95	1.34	1.09	0.25	1.28
C10'	41	31.4	9.6	29.44	1.34	1.25	0.09	1.44
C1"	22.1	26.97	4.87	24.84				
C2"	39.5	40.52	1.02	38.91	1.58	1.18	0.4	1.37
					1.9	1.25	0.65	1.44
C3"	19.5	21.64	2.14	19.3	1.63	1.51	0.12	1.7
C4"	41.2	42.57	1.37	41.03	1.48	1.63	0.15	1.82
C4"a	75	81.91	6.91	81.88				
C5"	116	115.53	0.47	116.8	6.57	6.3	0.28	6.56
C5"a	151.9	150.89	1.01	153.53				
C6"	129.4	126.7	2.7	128.4	6.89	6.65	0.24	6.92
C7"	132.2	131.57	0.63	133.46				
C8"	126.6	125.33	1.27	126.97	6.89	6.76	0.13	7.04
C8"a	120	123.46	3.46	125.04				
9"	23	27.37	4.37	25.25	2.64	2.47	0.17	2.68
9"a	48	46.49	1.51	45.11	1.65	1.55	0.1	1.74
10"	18.5	26.21	7.71	24.05	1.18	1.05	0.13	1.24
11"	33.1	31.75	1.35	29.8	0.93	0.83	0.1	1.01
12"	31	27.72	3.28	25.61	1.01	0.96	0.05	1.14

Table 7 NMR (δH and δC) experimental (Exp.), theoretical (DFT), and predicted (by linear models) data for dihydrochalcone **4B** (in ppm)

Position	Exp.	13C			Exp.	1H		
		Calc.	Res	Pred.		Calc.	Res	Pred.
C1	204.7	199.11	5.59	205.15				
C2	45.4	49.7	4.29	47.65	3.28	2.72	0.13	3.11
C3	30	32.65	2.65	29.69	2.85	2.87	0.41	2.95
C1'a	162.2	157.41	4.79	161.2				
C2'	75.6	79.25	3.65	78.81				
C3'	31.2	34.64	3.44	31.78	1.77	1.62	0.15	1.84
C4'	16.2	18.99	2.79	15.29	2.56	2.19	0.37	2.41
C4'a	100	100.18	0.18	100.87				
C5'	157	155.35	1.65	159.03				
C6'	104.8	108.07	3.27	109.19				
C7'	164.5	155.44	9.06	159.12				
C8'	94	93.98	0.02	94.33	5.87	5.59	0.28	5.87
C9'	25	24.19	0.81	20.77	1.34	1.13	0.21	1.34
C10'	41	31.41	9.59	28.38	1.34	1.28	0.06	1.49
C1"	22.1	40.65	18.55	38.12				
C2"	39.5	36.32	3.18	33.56	1.58	1.5	0.08	1.71
					1.9	1.08	0.82	1.28
C3"	19.5	24.77	5.27	21.38	1.63	1.55	0.08	1.77
C4"	41.2	34.93	6.27	32.09	1.48	1.94	0.46	2.16
C4"a	75	82.73	7.73	82.47				
C5"	116	114.54	1.46	116.01	6.57	6.3	0.27	6.59
C5"a	151.9	149.96	1.94	153.34				
C6"	129.4	126.46	2.94	128.57	6.89	6.67	0.22	6.97
C7"	132.2	132.47	0.27	134.91				
C8"	126.6	125.88	0.72	127.96	6.89	6.72	0.17	7.01
C8"a	120	121.97	1.97	123.84				
9"	23	29.16	6.16	26	2.64	1.86	0.78	2.08
9"a	48	50.6	2.6	48.61	1.65	1.21	0.44	1.42
10"	18.5	31.62	13.12	28.6	1.18	1.4	0.22	1.62
11"	33.1	33.07	0.03	30.13	0.93	0.74	0.27	0.94
12"	31	31.64	0.64	28.62	1.01	1.35	0.42	1.56

δ_C (Exp. – Calc.) in position C-10" = 7.71 ppm; residue related to δ_H (Exp. – Calc.) in position C-10" = 0.13 ppm and **4B** [residue related to δ_C (Exp. – Calc.) in position C-10" = 13.12 ppm residue related to δ_H (Exp. – Calc.) in position C-10" = 0.22 ppm (see Tables 6 and 7) showing that the structure **4A** has a theoretical value closer to the experimental one and that it possesses more-probable stereochemistry for the dihydrochalcone **4**.

Interactions between dihydrochalcones and cruzaine

To validate the accuracy of our docking protocol, the co-crystallized binder was docked back into the cruzaine enzyme. The root mean square deviation (RMSD) between the co-crystallized binder (blue) and the binding mode obtained by our docking protocol (orange) was 0.95 Å. As can be seen in Fig. S1, the two structures are quite overlapping, so the results were able to predict the experimental binding mode of the inhibitor at the catalytic site of cruzaine.

The results of the molecular docking study suggest good interaction between the non-covalent inhibitors and the active site of the enzyme. The results obtained from Mol-Dock Score are summarized in Table 8. Figure S2 simultaneously exhibits the four inhibitors docked in the binding pocket.

Figure 5 shows the docking positions of the dihydrochalcones **1**, **2**, **3**, and **4**, and also the residues involved in the molecular interaction.

The two compounds that showed the best inhibition values were the dihydrochalcones **1** and **4**. Compound **1** interacts with Ser61 and Cys25, and compound **4** interacts with several residues located in the catalytic site of the enzyme: Cys25, His161, and Asp160. These interactions are responsible for the stabilization and fixation of the inhibitor in the active site of cruzaine (Serafim et al. 2017). Cys25 and His161 are located in the subsite S1 and belong to the catalytic triad of the enzyme; these residues are important in the mechanism of enzymatic action (Arafet et al. 2017). Dihydrochalcones **2** and **3** establish hydrogen-bond interactions with Cys25 and Gly66, the latter being located in the S3 subsite of the enzyme.

Cys25 is the major residue related to the anti-*T. cruzi* activity. According to the mechanism proposed in the literature, interactions with these residues increase the inhibition of the enzyme. Our molecular docking results justify

Table 8 Molecular docking results

Inhibitor	MolDock score (kcal/mol)	Hydrogen bonds (kcal/mol)
Dihydrochalcone **1**	−139.43	−4.04
Dihydrochalcone **2**	−115.96	−5.70
Dihydrochalcone **3**	−119.62	−4.87
Dihydrochalcone **4**	−137.67	−6.67

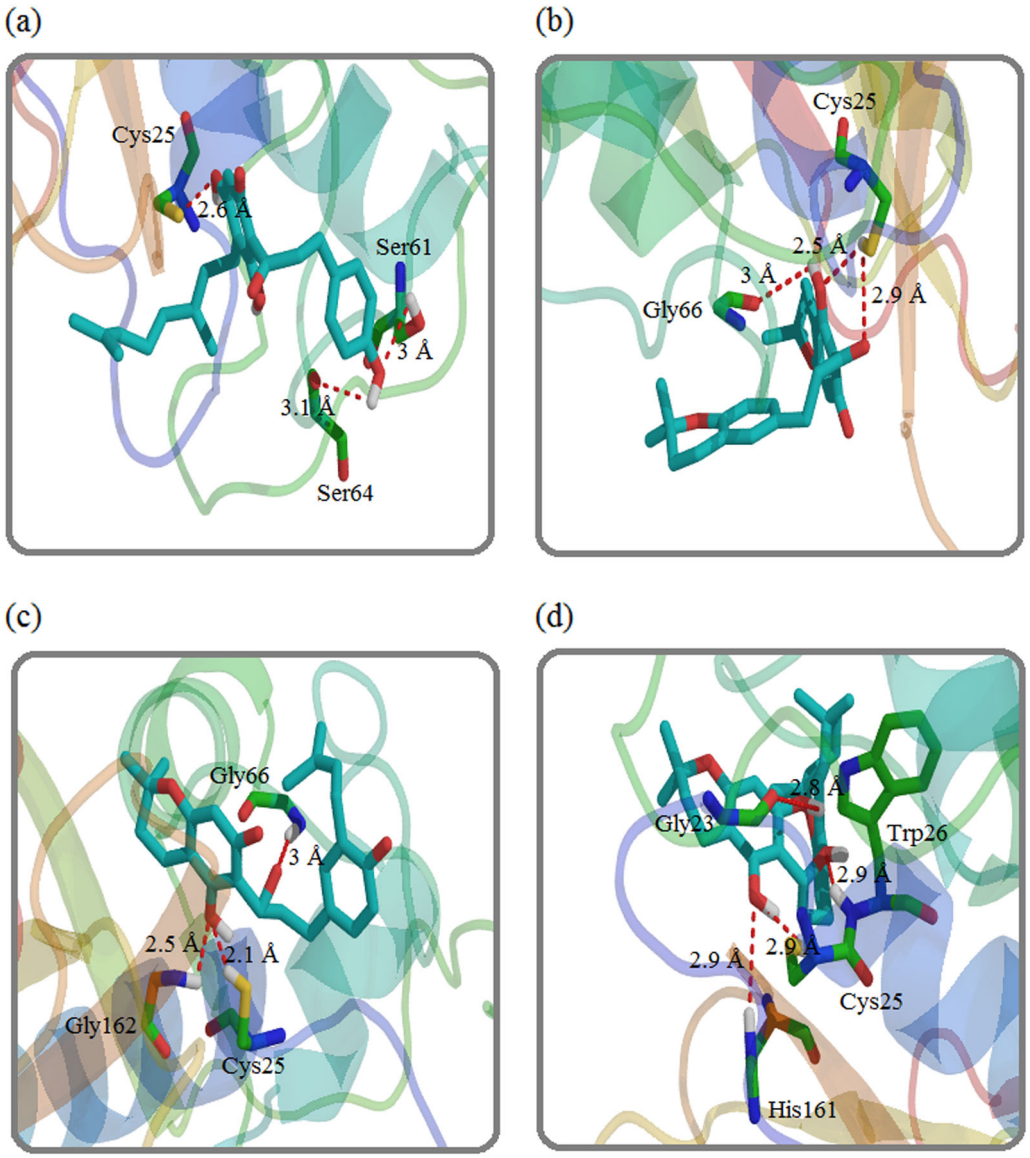

Fig. 5 Molecular interaction between dihydrochalcones and key catalytic residues

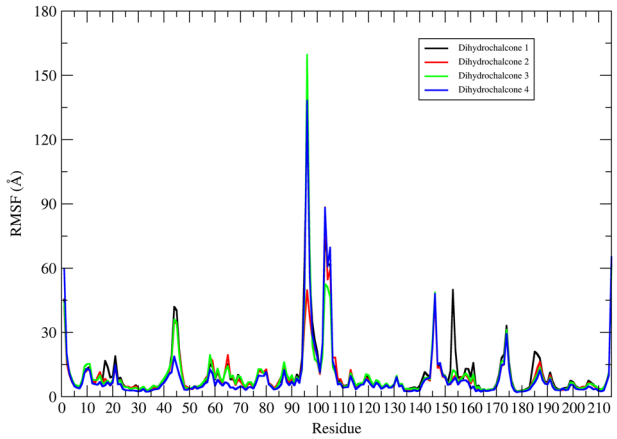

Fig. 6 Overlapping of RMSF graphs of the protein backbone

the great potential of these compounds to inhibit cruzaine and contribute to the studies of Burger et al. 2014.

Structural stability of the systems

The protein backbone fluctuation throughout the simulation time was analyzed, from the RMSF plots of alpha carbons versus the number of protein residues. In Fig. 6, the overlapping of the RMSF plots for the four systems can be observed.

In general, the graphs profile is similar, with some differences in the protein loop regions, however, these regions are structurally considered as being more flexible. This justifies the greater fluctuation observed in these residues, which were highlighted and can be seen in Fig. S3.

The stability of the cross-inhibitor systems was confirmed by the analysis of the RMSD plots during the 100 ns MD simulations.

Through the RMSD plots, in which the RMSD of the alpha carbon atoms versus the simulation time is displayed, it is possible to verify the stability and convergence of the protein backbone and the molecular structure of the inhibitors. For the inhibitors, only their heavy atoms were taken into consideration. Figure 7 shows the time series of the RMSD values for 100 ns of MD.

As can be seen in Fig. 7, the RMSDs of the protein backbone for all systems show that their structure remained stable, without significant conformational changes, during the simulation time. The dynamic evolution of the cross-linker structure was similar for all systems, with RMSD values of 0.96, 1.02, 0.83, and 0.79 for the systems where the receptor was complexed with molecules **1**, **2**, **3**, and **4**, respectively.

The structural stability of the ligands at the active site of the protein was also evaluated using the RMSD; the graphs for all inhibitors are shown in red color. Molecule **1** achieved structural stability after 40 ns; however, at about 80 ns, its RMSD underwent some oscillations; molecule **1** remained at the protein binding site for 100 ns. Inhibitor **2** showed conformational variability during the initial 50 ns and, only after 50 ns of simulation, it achieved conformational stability because of its interactions with the protein binding site residues. The highest conformational instability was observed for the third dihydrochalcone (several oscillations were observed in its RMSD plot); however, in the last 10 ns, the RMSD of this molecule showed tendency to reach an equilibrium. It is important to note that, despite this lack of stability, molecule **3** remained in the protein binding site.

Our fourth inhibitor was the one that most quickly reached a stable conformation. After approximately 10 ns and until the end of the MD simulation, the molecule showed the tendency to remain in a determined conformation, with rare small conformational deviations.

Binding affinity and energy components

To better understand the mode of interaction of these new inhibitors, it is important to estimate their binding affinities (ΔG_{bind}) and the values of the other energetic contributions. In this way, the MM-GBSA method was used to perform the free energy calculations and also to obtain the free energy results.

The ΔG_{bind} and the values of the van der Waals energetic (ΔE_{vdW}), electrostatic (ΔE_{ele}), polar (ΔG_{GB}), and nonpolar (ΔG_{nonpol}) contributions are summarized in Table 9.

The ΔG_{bind} for molecules **1**, **2**, **3**, and **4** were −28.73, −22.63, −24.68, and −26.18 kcal/mol, respectively. This ranking is in accordance with the experimental values proposed by Burger et al. (2014), which suggest the same classification for these compounds; the IC_{50} values are also present in Table 9.

The vdW contributions are the main factor responsible for the ligand–receptor interaction. In addition to the vdW energies, the ΔE_{ele} and ΔG_{npol} also favored this interaction. In all systems, the polar solvation free energy contribution counterbalances the favorable interactions.

Mode of interaction of the compounds with the cruzaine binding site

To evaluate the chemical interactions of the key residues in the receptor with the inhibitors, we used a per-residue free energy decomposition analysis.

Figure 8 summarizes the residues that perform interactions and the kind of interaction that exists between the protein and the different compounds.

As can be observed in Fig. 8, the interaction between the compounds and the protein is mainly due to the van der Waals contributions. In general, this is the preferential type

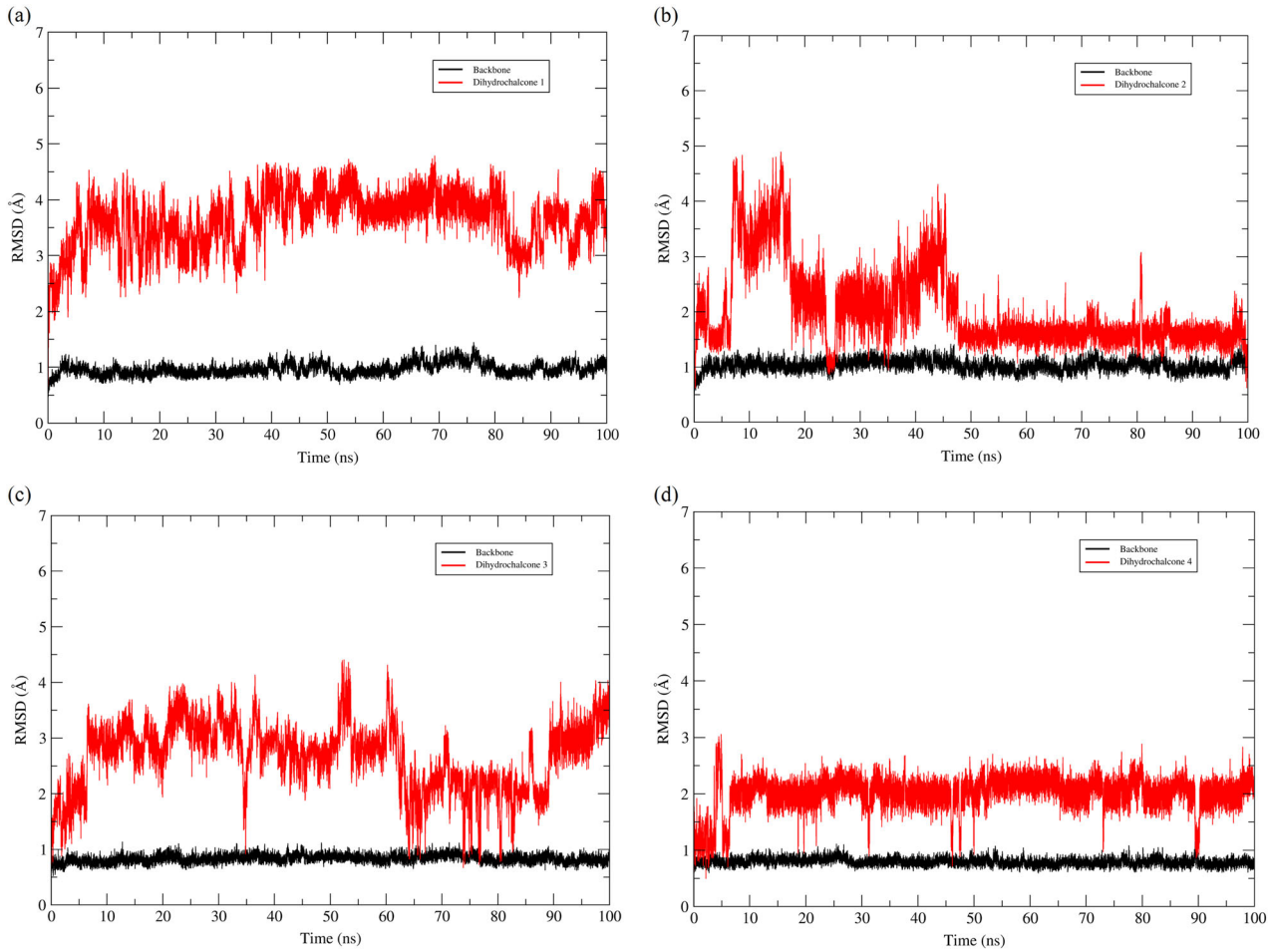

Fig. 7 RMSDs of the protein backbone (in black) and inhibitors (in red) (color figure online)

of interaction observed between the complexes under study and protein residues.

The inhibitors are observed to interact with residues other than those in the cruzaine binding site. The two best compounds reported by Burger et al. (2014) are dihydrochalcones **1** and **4**; the results of our per-residue analyses show that these molecules have different spectra of interaction with the amino acids in the binding cavity. This suggests that, during the MD simulation, the inhibitors moved inside the binding site and stabilized at slightly different positions. This movement occurred because the molecules sought satisfactory molecular interactions leading to the inhibition of the enzymatic activity.

Despite the fluctuations in the RMSD plot found for some inhibitors, all remained in their binding sites; however, to be accommodated in the catalytic pocket, the compounds had to undergo conformational changes.

The best binding pose for the first and fourth compounds was found to be deeply buried inside the catalytic site of the enzyme. The triphenol of compound **1** and the diphenol portion of compound **4** remained embedded in the catalytic site, which allowed the molecules to interact with the residues around it. The phenolic moiety of the inhibitor **1** and the cycloxane ring of molecule **4** were partially exposed to the solvent.

Molecules **2** and **3** do not have a long carbonic chain similar to that of the first inhibitor; instead, they have a bulky group formed by an oxane ring at the end of the chain and a shorter carbonic chain, respectively. Thus, these molecules performed few significant intermolecular interactions with the residues involved in the inhibition of cruzaine.

The strongest interaction between the first inhibitor and the protein occurs with Trp184 whereas, for the third inhibitor, it takes place with Leu67. Compounds **2** and **3** interact satisfactorily with few residues at the cruzaine binding site. This agrees with the low inhibition power found for these molecules.

The inhibition model of cysteine proteases (including cruzaine), according to the literature, reports that some compounds may inhibit the catalytic activity of these proteins interacting with subsites of the binding pocket, but not

Table 9 Estimated binding affinities and energetic contributions for the systems under study. The IC_{50} values obtained by Burger et al. (2014)

Compounds	ΔE_{vdW} (kcal/mol)	ΔE_{ele} (kcal/mol)	ΔG_{GB} (kcal/mol)	ΔG_{nonpol} (kcal/mol)	ΔG_{bind} (kcal/mol)	IC_{50} (μM)
Dihydrochalcone **1**	−28.65	−14.26	22.35	−8.17	−28.73	7.1 ± 0.2
Dihydrochalcone **2**	−25.41	−15.11	24.75	−6.86	−22.63	21.6 ± 2.5
Dihydrochalcone **3**	−27.39	−17.19	25.82	−5.92	−24.68	12.0 ± 0.1
Dihydrochalcone **4**	−27.32	−15.74	24.51	−7.63	−26.18	8.7 ± 2.0

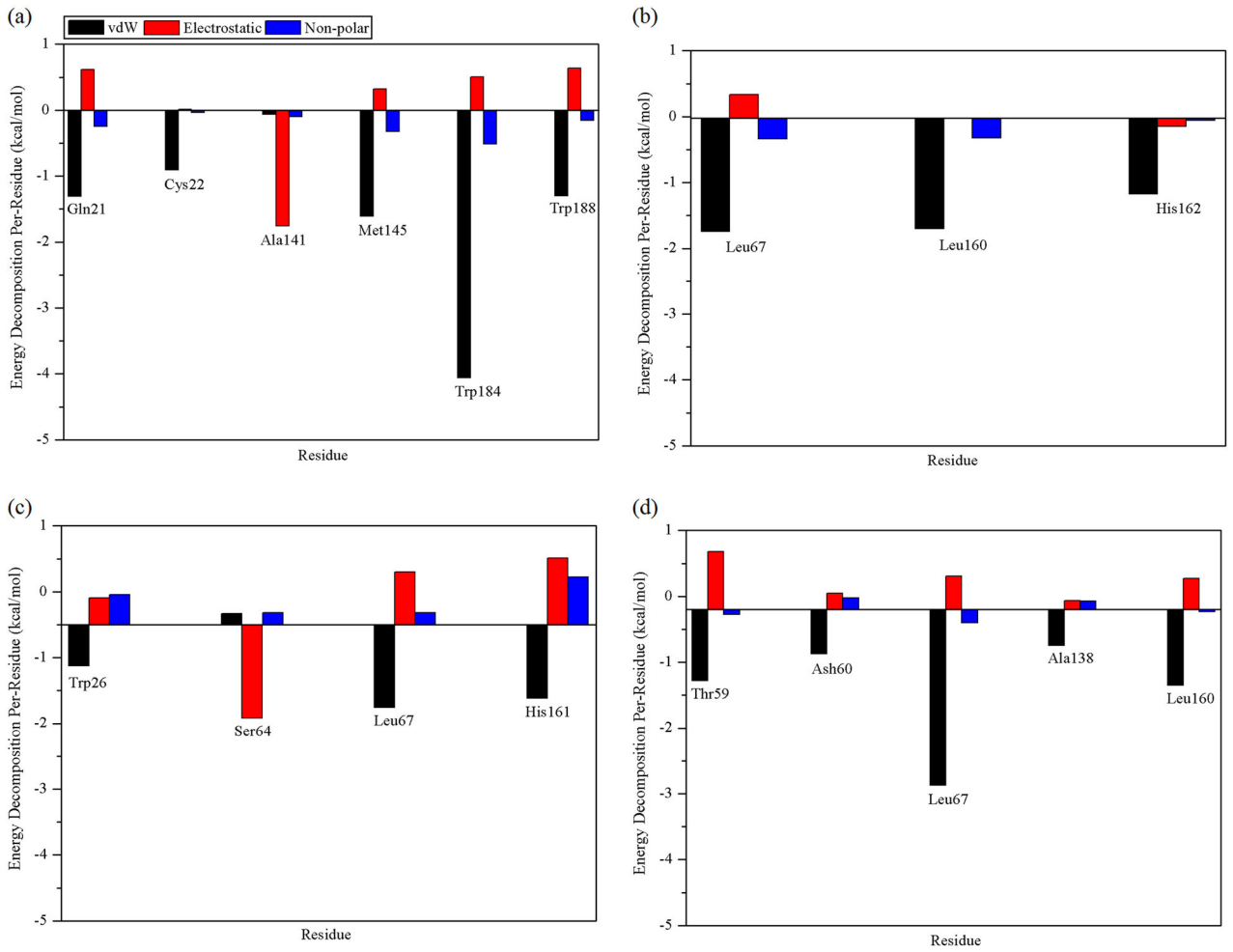

Fig. 8 Interactions between the inhibitors and the active pocket residues of cruzaine

necessarily with the residues belonging to the enzymatic catalytic triad. Thus, these inhibitors are able to inhibit substrate conversion by blocking their access to the protein binding pocket (Laskowski and Qasim 2000; Brak et al. 2008; Farady and Craik 2010; Wiggers et al. 2013). Our results suggest that the inhibitors that belong to the dihydrochalcones class have a mode of inhibition as described above, since they were able to remain bound to the active site of cruzaine throughout the time of MD dynamics. In addition, the experimental results of in vitro biological activity demonstrate the ability of the compounds under study to inhibit the cruzaine Burger et al. (2014).

Conclusions

The chemical shifts obtained for the nuclei of **1H** and **13C** using the DFT B3LYP/cc-pVDZ for structures **1**, **2**, and **3**

are consistent with the experimental ones, presenting low residues. Thus, the quantum method was used to elucidate structure **4**, which was not completely elucidated by traditional experimental techniques, making it possible to suggest that structure **4A** has more-probable stereochemistry for dihydrochalcone **4**. This indicates that the methodology used can be employed in studies of the prediction of spectroscopic properties of substances with structures similar to those described in this work.

In our molecular docking studies to predict the binding mode of the new inhibitors, it was possible to observe that these molecules are capable of interacting with residues important for the enzymatic activity like Cys25, His161, and Asp160. The amino acid residues Cys25 and His161 belong to the catalytic triad of cruzaine; therefore, the molecules that are capable of interacting with them have a high potential for inhibiting cruzaine. We also performed MD simulations to evaluate the molecular behavior of these inhibitors over time and free energy calculations with the MM/GBSA method. Our ΔG_{bind} results rank the inhibitors in accordance with the experimental results of Burger et al. (2014). The evaluation of the energy components involved in the ΔG_{bind} calculations demonstrated that the vdW interactions are the main factor responsible for the drug–receptor interactions.

Acknowledgements Jorddy N. Cruz appreciate the support of the Federal University of Pará and the National Council for Scientific and Technological Development (CNPq). Conflict of interest The authors declare that there is no conflict of interest regarding the publication of this paper.

Compliance with ethical standards

Conflict of interest The authors declare that they have no conflict of interest.

References

A Khan J, Wahab A, Javaid S, AL-Ghamdi M, Huwait E, Shaikh M, Shafqat A, Choudhary MI (2017) Studies on new urease inhibitors by using biochemical, STD-NMR spectroscopy, and molecular docking methods. Med Chem Res 26:2452–2467

Arafet K, Ferrer S, Moliner V (2017) Computational study of the catalytic mechanism of the cruzain cysteine protease. ACS Catal 7:1207–1215

Borges RS, Vale JKL, Pereira GAN, Veiga AAS, Junior JB, da Silva ABF, L Vale JK, N Pereira GA, S Veiga AA, Batista Jr. J, F da Silva AB (2016) An antioxidant mechanism of morphine and related derivatives. Med Chem Res 25:852–857

Brak K, Doyle PS, McKerrow JH, Ellman JA (2008) Identification of a new class of nonpeptidic inhibitors of cruzain. J Am Chem Soc 130:6404–6410

Brasil DSB, Alves CN, Guilhon GMSP, Muller AH, de S. Secco R, Peris G, Llusar R (2008) Crystal structure and theoretical study of IR and ^{1}H and ^{13}C NMR spectra of cordatin, a natural product with antiulcerogenic activity. Int J Quantum Chem 108:2564–2575

Burger MC, de M, Fernandes JB, da Silva MF, das GF, Escalante A, Prudhomme J, Le Roch KG, Izidoro MA, Vieira PC (2014) Structures and bioactivities of dihydrochalcones from *Metrodorea stipularis*. J Nat Prod 77:2418–2422

Caputto ME, Fabian LE, Benítez D, Merlino A, Ríos N, Cerecetto H, Moltrasio GY, Moglioni AG, González M, Finkielsztein LM (2011) Thiosemicarbazones derived from 1-indanones as new anti-Trypanosoma cruzi agents. Bioorg Med Chem 19:6818–26

Carneiro CM, Sánchez-Montalvá A, Corrêa-Oliveira R, Sales Jr. PA, Fonseca Murta SM, Salvador F, Molina I (2017) Experimental and clinical treatment of chagas disease: A review. Am J Trop Med Hyg 97:1289–1303

Case DA, Cheatham TE, Darden T, Gohlke H, Luo R, Merz KM, Onufriev A, Simmerling C, Wang B, Woods RJ (2005) The Amber biomolecular simulation programs. J Comput Chem 26:1668–1688

Chagas C, Chagas C (1909) Nova tripanozomiaze humana: estudos sobre a morfolojia e o ciclo evolutivo do Schizotrypanum cruzi n. gen., n. sp., ajente etiolojico de nova entidade morbida do homem. Mem Inst Oswaldo Cruz 1:159–218

Chatelain E (2017) Chagas disease research and development: Is there light at the end of the tunnel? Comput Struct Biotechnol J 15:98–103

Cimino P, Gomez-Paloma L, Duca D, Riccio R, Bifulco G (2004) Comparison of different theory models and basis sets in the calculation of 13C NMR chemical shifts of natural products. Magn Reson Chem 42:S26–S33

Cornell WD, Cieplak P, Bayly CI, Kollman PA (1993) Application of RESP charges to calculate conformational energies, hydrogen bond energies, and free energies of solvation. J Am Chem Soc 115:9620–9631

Coura JR (2015) The main sceneries of Chagas disease transmission. The vectors, blood and oral transmissions-a comprehensive review. Mem Inst Oswaldo Cruz 110:277–82

Cruz JN, Costa JFS, Khayat AS, Kuca K, Barros CAL, Neto AMJC (2018) Molecular dynamics simulation and binding free energy studies of novel leads belonging to the benzofuran class inhibitors of *Mycobacterium tuberculosis* polyketide synthase 13. J Biomol Struct Dyn 5:1–12

Darden T, York D, Pedersen L (1993) Particle mesh Ewald: An N ·log (N) method for Ewald sums in large systems. J Chem Phys 98:10089–10092

Dennington R, Keith TA, Millam JM (2015) GaussView Version 5 Semichem Inc., Shawnee Mission, KS.

Dolinsky TJ, Nielsen JE, McCammon JA, Baker NA (2004) PDB2PQR: an automated pipeline for the setup of Poisson-Boltzmann electrostatics calculations. Nucleic Acids Res 32: W665–W667

Farady CJ, Craik CS (2010) Mechanisms of macromolecular protease inhibitors. Chembiochem 11:2341–6

Frisch MJ, Trucks GW, Schlegel HB, Scuseria GE, Robb MA, Cheeseman JR, Scalmani G, Barone V, Mennucci B, Petersson GA, Nakatsuji H, Caricato M, Li X, Hratchian HP, Izmaylov AF, Bloino J, Zheng G, Sonnenberg JL, Hada M, Ehara M, Toyota K, Fukuda R, Hasegawa J, Ishida M, Nakajima T, Honda Y, Kitao O, Nakai H, Vreven T, Montgomery JA, Peralta JE, Ogliaro F, Bearpark M, Heyd JJ, Brothers E, Kudin KN, Staroverov VN, Kobayashi R, Normand J, Raghavachari K, Rendell A, Burant JC, Iyengar SS, Tomasi J, Cossi M, Rega N, Millam JM, Klene M, Knox JE, Cross JB, Bakken V, Adamo C, Jaramillo J, Gomperts R, Stratmann RE, Yazyev O, Austin AJ, Cammi R, Pomelli C, Ochterski JW, Martin RL, Morokuma K, Zakrzewski VG, Voth GA, Salvador P, Dannenberg JJ, Dapprich S, Daniels

AD, Farkas, Foresman JB, Ortiz JV, Cioslowski J, Fox DJ (2009) Gaussian 09, Revision B.01. Gaussian, Inc., Wallingford, CT

Gauss J, Stanton JF (1995) Gauge-invariant calculation of nuclear magnetic shielding constants at the coupled–cluster singles and doubles level. J Chem Phys 102:251–253

Genheden S, Ryde U (2015) The MM/PBSA and MM/GBSA methods to estimate ligand-binding affinities. Expert Opin Drug Discov 10:449–461

Gohlke H, Kiel C, Case DA (2003) Insights into protein-protein binding by binding free energy calculation and free energy decomposition for the Ras-Raf and Ras-RalGDS complexes. J Mol Biol 330:891–913

Huang L, Brinen LS, Ellman JA (2003) Crystal structures of reversible ketone-Based inhibitors of the cysteine protease cruzain. Bioorg Med Chem 11:21–29

Izaguirre JA, Catarello DP, Wozniak JM, Skeel RD (2001) Langevin stabilization of molecular dynamics. J Chem Phys 114:2090–2098

Jorgensen WL, Chandrasekhar J, Madura JD, Impey RW, Klein ML (1983) Comparison of simple potential functions for simulating liquid water. J Chem Phys 79:926–935

Kaur K, Kumar V, Beniwal V, Kumar V, Aneja KR, Sharma V, Jaglan S (2015) Solvent-free synthesis of novel (E)-2-(3,5-dimethyl-4-(aryldiazenyl)-1H-pyrazol-1-yl)-4-arylthiazoles: determination of their biological activity. Med Chem Res 24:3863–3875

Kollman PA, Massova I, Reyes C, Kuhn B, Huo S, Chong L, Lee M, Lee T, Duan Y, Wang W, Donini O, Cieplak P, Srinivasan J, Case DA, Cheatham TE (2000) Calculating structures and free energies of complex molecules: combining molecular mechanics and continuum models. Acc Chem Res 33:889–97

Laskowski M, Qasim MA (2000) What can the structures of enzyme-inhibitor complexes tell us about the structures of enzyme substrate complexes? Biochim Biophys Acta-Protein Struct Mol Enzymol 1477:324–337

Lee C, Yang W, Parr RG (1988) Development of the Colle-Salvetti correlation-energy formula into a functional of the electron density. Phys Rev B Condens Matter 37:785–789

Magalhaes Moreira DR, de Oliveira ADT, Teixeira de Moraes Gomes PA, de Simone CA, Villela FS, Ferreira RS, da Silva AC, dos Santos TAR, Brelaz de Castro MCA, Pereira VRA, Leite ACL (2014) Conformational restriction of aryl thiosemicarbazones produces potent and selective anti-Trypanosoma cruzi compounds which induce apoptotic parasite death. Eur J Med Chem 75:467–478

Maier JA, Martinez C, Kasavajhala K, Wickstrom L, Hauser KE, Simmerling C (2015) ff14SB: Improving the accuracy of protein side chain and backbone parameters from ff99SB. J Chem Theory Comput 11:3696–3713

Massarico Serafim RA, Gonçalves JE, de Souza FP, de Melo Loureiro AP, Storpirtis S, Krogh R, Andricopulo AD, Dias LC, Ferreira EI (2014) Design, synthesis and biological evaluation of hybrid bioisoster derivatives of N-acylhydrazone and furoxan groups with potential and selective anti-Trypanosoma cruzi activity. Eur J Med Chem 82:418–425

McGrath ME, Eakin AE, Engel JC, McKerrow JH, Craik CS, Fletterick RJ (1995) The crystal structure of cruzain: A therapeutic target for Chagas' disease. J Mol Biol 247:251–259

Miertuš S, Scrocco E, Tomasi J (1981) Electrostatic interaction of a solute with a continuum. A direct utilizaion of AB initio molecular potentials for the prevision of solvent effects. Chem Phys 55:117–129

Moreira RYO, Brasil DSB, Alves CN, Guilhon GMSP, Santos LS, Arruda MSP, Müller AH, Barbosa PS, Abreu AS, Silva EO, Rumjanek VM, Souza J, da Silva ABF, Santos RH, de A (2008) Crystal structure and theoretical calculations of Julocrotine, a natural product with antileishmanial activity. Int J Quantum Chem 108:513–520

Morillo CA, Marin-Neto JA, Avezum A, Sosa-Estani S, Rassi A, Rosas F, Villena E, Quiroz R, Bonilla R, Britto C, Guhl F, Velazquez E, Bonilla L, Meeks B, Rao-Melacini P, Pogue J, Mattos A, Lazdins J, Rassi A, Connolly SJ, Yusuf S (2015) Randomized trial of benznidazole for chronic chagas' cardiomyopathy. N Engl J Med 373:1295–1306

Pérez-Molina JA, Molina I (2018) Chagas disease. Lancet (Lond, Engl) 391:82–94

Rauhut G, Puyear S, Wolinski K, Pulay P (1996) Comparison of NMR shieldings calculated from Hartree−Fock and density functional wave functions using gauge-including atomic orbitals. J Phys Chem 100:6310–6316

Ryckaert JP, Ciccotti G, Berendsen HJC (1977) Numerical integration of the cartesian equations of motion of a system with constraints: molecular dynamics of n-alkanes. J Comput Phys 23:327–341

Serafim RAM, de Oliveira TF, Loureiro APM, Krogh R, Andricopulo AD, Dias LC, Ferreira EI (2017) Molecular modeling and structure–activity relationships studies of bioisoster hybrids of N-acylhydrazone and furoxan groups on cruzain. Med Chem Res 26:760–769

Thomsen R, Christensen MH (2006) MolDock: A new technique for high-accuracy molecular docking. J Med Chem 49:3315–3321

Turk D, Guncar G, Podobnik M, Turk B (1998) Revised definition of substrate binding sites of papain-like cysteine proteases. Biol Chem 379:137–47

Wang J, Cieplak P, Kollman PA (2000) How well does a restrained electrostatic potential (RESP) model perform in calculating conformational energies of organic and biological molecules? J Comput Chem 21:1049–1074

Wang J, Wolf RM, Caldwell JW, Kollman PA, Case DA (2004) Development and testing of a general amber force field. J Comput Chem 25:1157–1174

Wiggers HJ, Rocha JR, Fernandes WB, Sesti-Costa R, Carneiro ZA, Cheleski J, da Silva ABF, Juliano L, Cezari MHS, Silva JS, McKerrow JH, Montanari CA (2013) Non-peptidic cruzain inhibitors with trypanocidal activity discovered by virtual screening and in vitro assay. PLoS Negl Trop Dis 7:e2370

Wild DJ (2005) MINITAB Release 14. J Chem Inf Model 45:212